inorganics

MDPI

Article

A First-Principle Study of Two-Dimensional Boron Nitride Polymorph with Tunable Magnetism

Liping Qiao [1], Zhongqi Ma [1], Fulong Yan [1], Sake Wang [2] and Qingyang Fan [3,*]

[1] Team of Micro & Nano Sensor Technology and Application in High-Altitude Regions, School of Information Engineering, Xizang Minzu University, Xianyang 712082, China; lpqiao@126.com (L.Q.); mazhongqi_my@163.com (Z.M.); yanfulong_xzmu@163.com (F.Y.)
[2] College of Science, Jinling Institute of Technology, Nanjing 211169, China; isaacwang@jit.edu.cn
[3] College of Information and Control Engineering, Xi'an University of Architecture and Technology, Xi'an 710055, China
* Correspondence: qyfan_xidian@163.com

Abstract: Using the first-principles calculation, two doping two-dimensional (2D) BN (boron nitride) polymorphs are constructed in this work. The two doping 2D BN polymorphs B_5N_6Al and B_5N_6C sheets are thermally stable under 500 K. All the B_6N_6, B_5N_6Al, and B_5N_6C sheets are semiconductor materials with indirect band gaps on the basis of a hybrid functional. The anisotropic calculation results indicate that Young's modulus (E) and Poisson's ratio (v) of the B_6N_6, B_5N_6Al, and B_5N_6C sheets are anisotropic in the xy plane. In addition, the magnetic properties of the B_6N_6, B_5N_6Al, and B_5N_6C sheets have also been investigated. According to the calculation of the magnetic properties, B_6N_6 sheet does not exhibit magnetism, while it shows weak magnetism after doping carbon atom to the BN sheet. This paper explores the influence mechanism of doping different atoms on the basic physical properties of two-dimensional BN sheets. It not only constructs a relationship between structure and performance but also provides theoretical support for the performance regulation of BN materials.

Keywords: two-dimensional (2D) BN sheet; electronic band structure; density of states; anisotropic properties; magnetism

Citation: Qiao, L.; Ma, Z.; Yan, F.; Wang, S.; Fan, Q. A First-Principle Study of Two-Dimensional Boron Nitride Polymorph with Tunable Magnetism. *Inorganics* **2024**, *12*, 59. https://doi.org/10.3390/inorganics12020059

Academic Editor: Jean-François Halet

Received: 25 December 2023
Revised: 30 January 2024
Accepted: 30 January 2024
Published: 15 February 2024

1. Introduction

Graphene is a planar 2D carbon allotrope with single atomic thickness. Due to its special electronic and magnetic characteristics, graphene is considered to be a revolutionary material for multiple facilities, such as high-speed electronic devices, thermal and conductivity-enhancing composite materials, sensors, RF logic devices, transparent electrodes, etc. [1–6]. In recent years, novel theoretical two-dimensional materials based on first-principles calculations have shown many interesting physical and chemical properties [7–12]. As isoelectronic bodies, BN and carbon also have rich and colorful physical properties and polymorphs [13–18].

Research on low-dimensional boron nitride nanomaterials is important in the field of materials science [19–24], especially because their excellent chemical properties and thermal stability have been widely studied [25]. They can enhance the mechanical enhancement and thermal conductivity of various crystal structures, for instance, polymers, ceramics, and metals [26–28]. Research has shown that graphene-like h-BN sheets have remarkable electronic and optical characteristics [29] and show a wide band gap and intense absorption capacity in the ultraviolet region. In other studies in the literature, it was shown that at low doping rates, B-N prefers to replace *sp* hybrid carbon on the chain than hexagonal. At high doping rates, it first attacks the hexagonal structure and then the chain.

Qi et al. [30] predicted 2D BxNy ($1 < x/y \leq 2$) sheets using the density functional theory (DFT) [31,32]. B_5N_3 and B_7N_5 sheets possess enough low enthalpy of formation

and outstanding dynamic stability, which makes them possible to be found in experiments. Unlike previous BN, both B_5N_3 and B_7N_5 sheets exhibit narrow band gaps of 1.99 eV and 2.40 eV, respectively. Two-dimensional orthorhombic boron nitride crystal, named o-B_2N_2, was designed by Demirci et al. [23]. The stability of o-B_2N_2 at room temperature and ambient pressure has been confirmed. o-B_2N_2 is a semiconductor with a direct band gap of 1.70 eV. An appropriate band gap makes this structure exhibit higher light absorption in the visible light range along the armchair direction. The in-plane stiffness of o-B_2N_2 is also very close to that of hexagonal BN. Based on the DFT, Fan et al. [33] first proposed and studied in detail a new 2D *Pmma*-BN sheet. The stability of *Pmma*-BN sheet was demonstrated by phonon spectroscopy and ab initio molecular dynamics simulations at 300 and 500 K. Uniaxial strain has weakened the *ZT* of the *Pmma*-BN sheet and led to a decrease in thermoelectric conversion efficiency. Anota et al. [34] reported boron nitride nanosheets containing homonuclear boron bonds and found that the proportion of boron atoms in nanosheets is related to conductivity.

By inserting *sp*-hybridized BN bonds into a monolayer h-BN structure, Li et al. [24] designed BNyne, Bndiyne, and BNtriyne. To explore the influence mechanism on the physical properties of doped 2D boron nitride, B_6N_6 sheets (called BNyne in ref. [24]) with doping Al or C atoms are proposed in this work, named B_5N_6Al sheet and B_5N_6C sheet, respectively. Both carbon and aluminum have the advantages of being cheap and easy to obtain. The doping of C element is selected to improve the mechanical properties of B_6N_6, and the selection of Al element is to observe the influence of metal elements on the electrical properties of semiconductor materials. We verify the structural stability of B_5N_6Al sheet and B_5N_6C sheet from mechanical and thermal perspectives and study their elementary physical characteristics based on first-principles calculations. B_5N_6Al and B_5N_6C are both indirect band gap semiconductor materials, which are the same as B_6N_6. The band gap width of B_5N_6C is significantly reduced. More importantly, the spin-up and spin-down electronic band structures indicate that B_6N_6 sheet does not exhibit magnetism. But after adding carbon to the BN sheet, it changes from a nonmagnetic material to a magnetic material.

2. Results and Discussion

Two-dimensional boron nitride structures and the crystal structure model doped with aluminum and carbon atoms are shown in Figure 1, together with the configurations of h-BN, o-B_2N_2 [23], B_5N_3 [30], and B_7N_5 [30]. Here, light blue, light pink, green, and light red represent boron atoms, nitrogen atoms, aluminum atoms, and carbon atoms, respectively. h-BN is a hexagonal network-layered crystal composed of nitrogen atoms and boron atoms; its layered structure is similar to graphite. oB_2N_2 is a two-dimensional monolayer of boron nitride in an orthorhombic structure with a B-B and N-N double-atom structure. h-BN and oB_2N_2 are only composed of six-membered rings, while the crystal structure of B_5N_3 is composed of seven-membered rings and five-membered rings. B_7N_5 contains seven-membered rings, six-membered rings, and five-membered rings. By inserting B-N bonds into h-BN sheet, Li et al. [24] proposed two-dimensional B_6N_6, as shown in Figure 1. After being fully optimized, all of them—B_6N_6 sheet, B_5N_6Al sheet, and B_5N_6C sheet—retain their planar structure. All the unit cells of three B_6N_6, B_5N_6Al, and B_5N_6C sheets contain twelve atoms. The boron and nitrogen atoms in B_6N_6 sheet are half the same, and the other two doping models replace one B atom.

The lattice parameters of the three B_6N_6, B_5N_6Al, and B_5N_6C sheets are listed in Table 1. The optimized lattice parameter of B_6N_6 is a = 6.20 Å. After doping with Al and C atoms, the symmetry of the crystal structure changes, and the lattice parameters a and b of B_5N_6Al and B_5N_6C are no longer equal. In B_6N_6 sheet structure, due to the larger radius of aluminum atoms, the lattice parameters of B_5N_6Al increase, while the lattice parameters of B_5N_6C do not change much. However, the radius difference between carbon atoms, boron atoms, and nitrogen atoms is not significant.

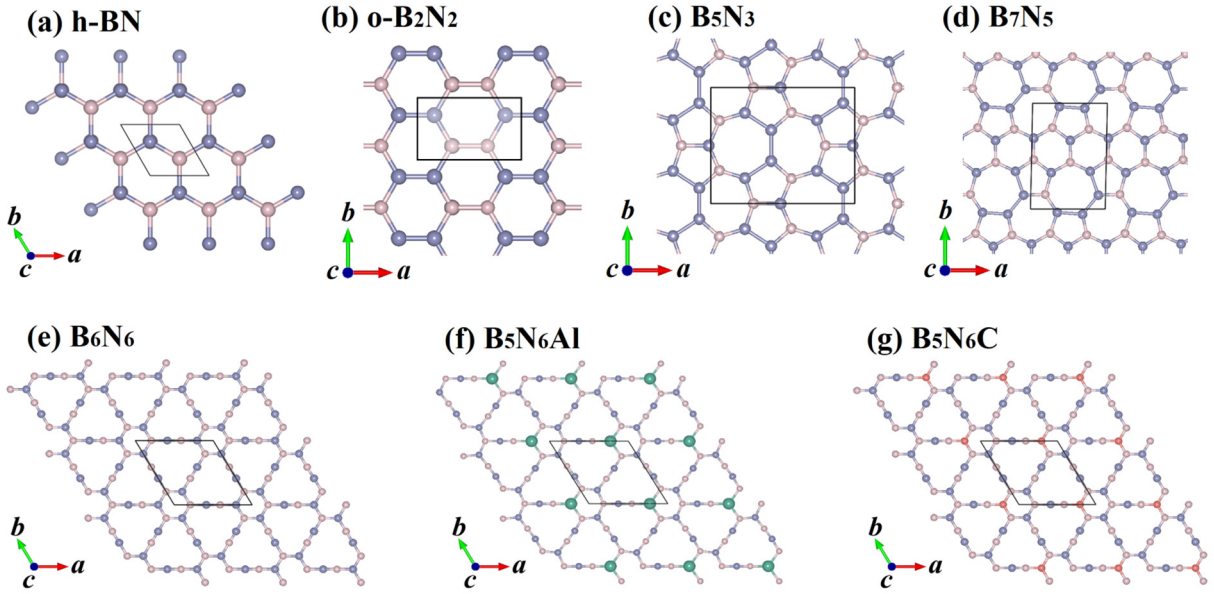

Figure 1. Crystal structures of the h-BN (**a**), o-B_2N_2 (**b**), B_5N_3 (**c**), B_7N_5 (**d**), B_6N_6 (**e**), B_5N_6Al (**f**), and B_5N_6C (**g**). Light blue, light pink, green, and light red represent boron atoms, nitrogen atoms, aluminum atoms, and carbon atoms, respectively.

Table 1. Lattice constant (Å) and bond length (Å) of B_6N_6, B_5N_6Al, and B_5N_6C.

	a	*b*	b1	b2	b3	b4	b5	b6
B_6N_6	6.20		1.275	1.278	1.094			
B_5N_6Al	7.40	7.18	1.796	1.451	1.465	1.390	1.264	1.374
B_5N_6C	6.86	5.93	1.381	1.451	1.441	1.380	1.260	1.391

The decrease in lattice parameters is caused by structural distortion in the six-membered ring in the structure, and the details of this are shown in Figure 2. The bond lengths of B_6N_6, B_5N_6Al, and B_5N_6C sheets are also listed in Table 1. The doping of atoms makes the bond lengths in both B_5N_6Al and B_5N_6C sheets increase to six different bond lengths, which is three more than in B_6N_6 sheet, and the angles of the six-membered ring have also become irregular. In B_6N_6 sheet, the bond length of the six-membered ring is uniform, the bond angle is 120°, the maximum bond length is 1.278 Å, and the shortest bond length is 1.094 Å. For B_5N_6Al sheet, the six-membered ring has undergone serious distortion, and the bond angle and bond length have changed. The maximum bond length of B_5N_6Al is 1.796 Å, which is approximately 41% higher than that of B_6N_6. The shortest bond length is 1.264 Å. Regarding B_5N_6C sheet, the six-membered ring has a small degree of distortion, and the maximum bond length is 1.451 Å, which is approximately 14% longer than that of B_6N_6, and the shortest bond length is 1.260 Å.

Ab initio molecular dynamic (AIMD) simulations were performed to evaluate the thermal stabilities of B_5N_6Al and B_5N_6C sheets under 500 K. The supercell of B_5N_6Al and B_5N_6C sheets before and after 5 ps simulation at a temperature of 500 K is also shown in Figure 3. The supercells of B_5N_6Al and B_5N_6C did not change significantly, and the B-N, N-Al and B-C bonds were not broken. The total energy fluctuation was also maintained at a stable level, indicating that B_5N_6Al and B_5N_6C have thermal stability at 500 K.

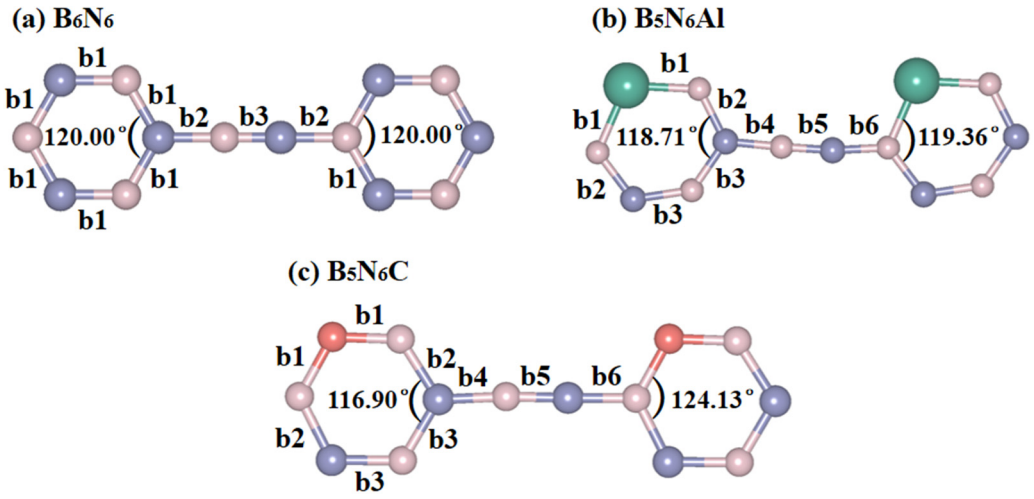

Figure 2. The bond length and bond angle of B_6N_6 (**a**), B_5N_6Al (**b**), and B_5N_6C (**c**).

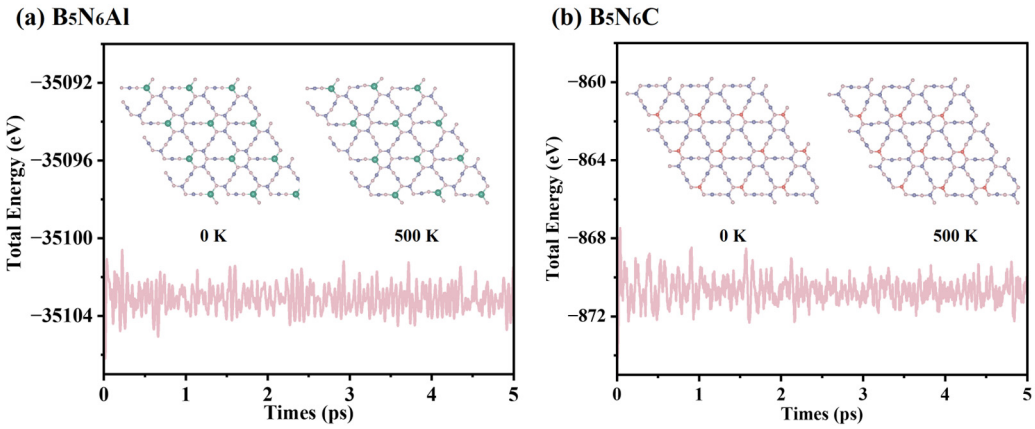

Figure 3. Total energy fluctuations of B_5AlN_6 and B_5N_6C as a function of the AIMDs simulation at 500 K.

The mechanical stability of B_6N_6, B_5N_6Al, and B_5N_6C sheets was also estimated, and the mechanical stability was evaluated by estimating the elastic constant. For 2D materials, the elastic constants can be obtained by the energy–strain method. That is, by applying different strains to the structure, the total energy of the system relative to the ground state energy change can be calculated. The relationship between the strain and the resulting energy change is expressed as [35]:

$$E(\varepsilon) - E_0 = \frac{1}{2}C_{11}\varepsilon_{xx}^2 + \frac{1}{2}C_{22}\varepsilon_{yy}^2 + C_{12}\varepsilon_{xx}\varepsilon_{yy} + 2C_{44}\varepsilon_{xy}^2 \quad (1)$$

where E_0 and $E(\varepsilon)$ represent the ground state configuration and total energy after strain application, respectively. ε denotes the strain; xx and yy denote the direction. By fitting the energy curve corresponding to the strain, C_{11}, C_{22}, C_{12}, and C_{44} as elastic constants can be obtained. The Born–Huang criteria [36] are a necessary condition for the elastic constants of 2D materials with mechanical stability, that is, $C_{11}C_{22} - C_{12}^2 > 0$ and $C_{44} > 0$. The elastic constants of B_6N_6, B_5N_6Al, and B_5N_6C sheets are shown in Table 2, which obviously meet the mechanical stability conditions. The $C_{11} = C_{22} = 180.98$ N/m of B_6N_6, which is lower than that of h-BN ($C_{11} = C_{22} = 290$ N/m [37]) and *pmma* BN ($C_{11} = 195$ N/m, $C_{22} = 256$ N/m).

Table 2. Elastic constants C_{ij} (N/m), Young's modulus E (N/m), and Poisson's ratio v of B_6N_6, B_5N_6Al, and *P*-62*m* B_5N_6C.

	C_{11}	C_{12}	C_{22}	C_{66}	E_x	E_y	v_x	v_y
B_6N_6	180.98	82.09	180.98	49.45	141.18	141.18	0.46	0.46
B_5N_6Al	152.14	86.84	126.11	44.78	97.83	76.19	0.69	0.57
B_5N_6C	201.78	103.48	204.66	53.35	149.46	151.59	0.50	0.51

Compared with B_6N_6, the C_{11} of B_5N_6Al is reduced by approximately 16%, and the C_{22} is reduced by approximately 30%, which indicates that the ability to resist deformation along the x and y directions is weakened. That is, the Al atom plays a weakening role in the mechanical properties of B_6N_6. However, the addition of carbon atoms leads to an improvement in mechanical properties. The elastic constants C_{11} and C_{22} of B_5N_6C are increased by approximately 12~13%. Young's modulus along the x and y directions E_x and E_y of B_5N_6C is also greater than that of B_6N_6, which may be due to the fact that carbon atoms are more likely to form stable covalent bonds. With the addition of aluminum and carbon atoms, B_5N_6Al and B_5N_6C sheets have lower and higher elastic constants than B_6N_6 sheets, respectively. Thus, the doping of carbon and aluminum atoms has different influence mechanisms on the mechanical properties of B_6N_6 sheets. The former significantly improves the elastic constants and elastic modulus, while the latter weakens the ability of B_6N_6 sheets to resist deformation and makes them easier to compress. Poisson's ratios of B_5N_6Al and B_5N_6C sheets are 0.69 and 0.50 along the x-axis and 0.57 and 0.51 along the y-axis, respectively, which are higher than those of B_6N_6 sheets.

On the basis of the elastic constants, the in-plane E and v along any direction θ can be taken as [35]:

$$E(\theta) = \frac{C_{11}C_{22} - C_{12}^2}{C_{11}\alpha^4 + C_{22}\beta^4 + (\frac{C_{11}C_{22} - C_{12}^2}{C_{44}} - 2C_{12})\alpha^2\beta^2} \quad (2)$$

$$v(\theta) = -\frac{(C_{11} + C_{22} - \frac{C_{11}C_{22} - C_{12}^2}{C_{44}})\alpha^2\beta^2 - C_{12}(\alpha^4 + \beta^4)}{C_{11}\alpha^4 + C_{22}\beta^4 + (\frac{C_{11}C_{22} - C_{12}^2}{C_{44}} - 2C_{12})\alpha^2\beta^2} \quad (3)$$

where $\alpha = \sin\theta$; $\beta = \cos\theta$. In order to further explore the effect of carbon and aluminum atoms doping on the elastic anisotropy of B_6N_6 sheets, the angle-dependent in-plane E and v of B_6N_6, B_5N_6Al, and B_5N_6C sheets are illustrated in Figure 4. Further, 0° and 90° represent the directions of orthorhombic unit cells along the x- and y-axes, respectively. With the addition of aluminum, the maximum value of the E of B_5N_6Al sheet is lower than that of B_6N_6 sheet, but the minimum value is greater than that of B_6N_6 sheet, while the E of B_5N_6C sheet is larger than that of B_6N_6 sheet, and it shows an in-plane stiffness superior to B_6N_6 sheet. For Poisson's ratio, B_6N_6 sheet has a higher Poisson ratio than that of B_5N_6Al and B_5N_6C sheet, indicating that B_6N_6 sheet is more likely to expand laterally than B_5N_6Al and B_5N_6C sheet when tension is applied. The smallest in-plane Poisson's ratio of B_6N_6, B_5N_6Al, and B_5N_6C sheets occurs along the x-axis. When they are stretched diagonally, a maximum value occurs.

The orientation dependence of 2D Young's modulus is closer to the sphere, indicating that the weaker the anisotropy, the smaller the difference between the maximum and minimum values. On the contrary, the more it deviates from the spherical shape, the stronger the anisotropy. The minimum value of Young's modulus of B_6N_6 is 2.36 N/m, and the maximum value is 144 N/m, showing strong anisotropy. The minimum value of Young's modulus of B_5N_6Al is 4.63 N/m, and the maximum value is 92 N/m; anisotropy is weakened compared with B_6N_6. The minimum Young's modulus of B_5N_6C is 59 N/m, and the maximum is 152 N/m, showing the weakest Young's modulus anisotropy. The ratio of the maximum to minimum Young's modulus of B_6N_6, B_5N_6Al, and B_5N_6C sheets is 60.91, 19.94, and 2.57, respectively. These values clearly and intuitively show the influence of atomic doping on the anisotropy of Young's modulus. Both carbon atoms and

aluminum atoms can weaken anisotropy, especially when the effect of carbon atoms is more significant. The ratio of the 2D extreme values of Poisson's ratio of B_6N_6, B_5N_6Al, and B_5N_6C sheets is 2.2, 1.72, and 1.60, respectively, indicating that the order of Poisson's ratio anisotropy is B_6N_6 > B_5N_6Al > B_5N_6C, which is consistent with the order of anisotropy of Young's modulus.

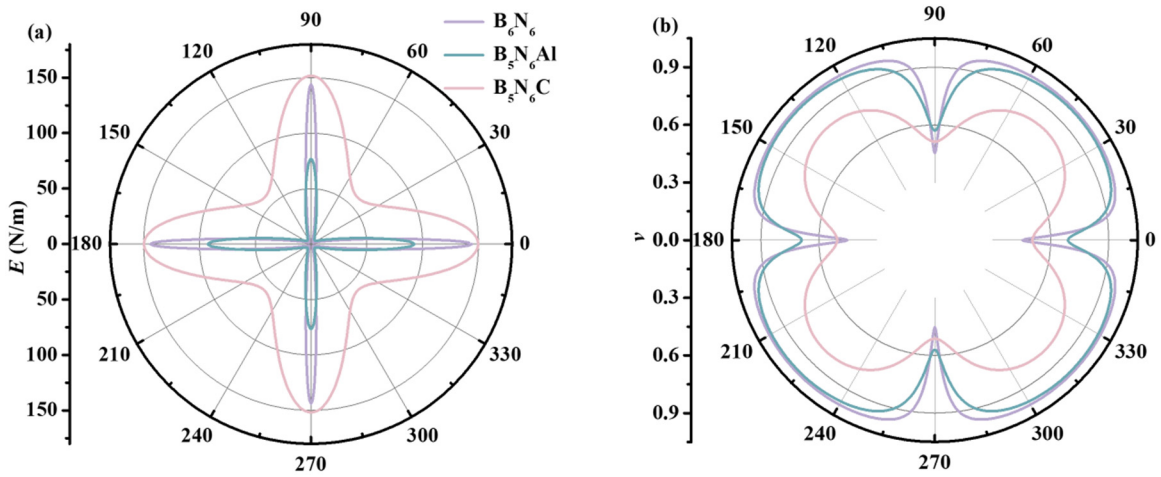

Figure 4. Orientation dependencies of Young's modulus (**a**) and Poisson's ratio (**b**) for B_6N_6, B_5N_6Al, and B_5N_6C.

In addition to in-plane stiffness, the stress neutralization of B_6N_6, B_5N_6Al, and B_5N_6C sheets under uniaxial strain is further analyzed, and the detailed results are presented in Figure 5. The ultimate strength of B_6N_6 sheet is 18.49 N/m loaded along the x (y)-axis with 19.5% uniaxial strain, while with the addition of aluminum atoms, although the ultimate strength has decreased slightly, the strain along the x-axis is not significantly different (18.5%). The x- and y-axis of B_5N_6C sheet have similar and good uniaxial strain limitations. The ultimate strength along the x- and y-axis of B_5N_6C sheet under the calculated maximum strength is 17.0%, respectively. For B_5N_6C sheet, the ultimate strength is 18.14 N/m and 18.50 N/m along the x or y direction, respectively. Therefore, B_6N_6 sheet and B_6N_6 sheet doped with carbon atom have good mechanical properties compared to B_5N_6Al sheet, which may be suitable for nanomechanical applications.

The band structures of the B_6N_6, B_5N_6Al, and B_5N_6C sheets are shown in Figure 6. The related results show that all the B_6N_6, B_5N_6Al, and B_5N_6C sheets exhibit semiconductor characters, and the band gaps of B_6N_6 and B_5N_6Al sheets are 5.684 and 5.418 eV, respectively. After doping with Al atoms, the variation in the band gap of B_5N_6Al sheet is relatively small, while after doping the C atoms, the change in the band gap of B_5N_6C sheet is significant. To study the magnetism of these materials, we also calculated spin-up and spin-down band structures of B_6N_6, B_5N_6Al, and B_5N_6C sheets. From the band structures analysis, there is no difference between spin-up and spin-down for B_6N_6 and B_5N_6Al sheets, which indicates that they do not conform to the characteristics of magnetic materials. Nevertheless, after doping with carbon atoms, there is a significant difference in the band structure of spin-up and spin-down. The conduction band minimum (CBM) and valence band maximum (VBM) of the spin-up band structure are located at the X and Γ points, respectively, with a wide indirect band gap of 5.181 eV, while the CBM and VBM of the -up appear at the Y and X points, with the narrow band gap being only 1.062 eV.

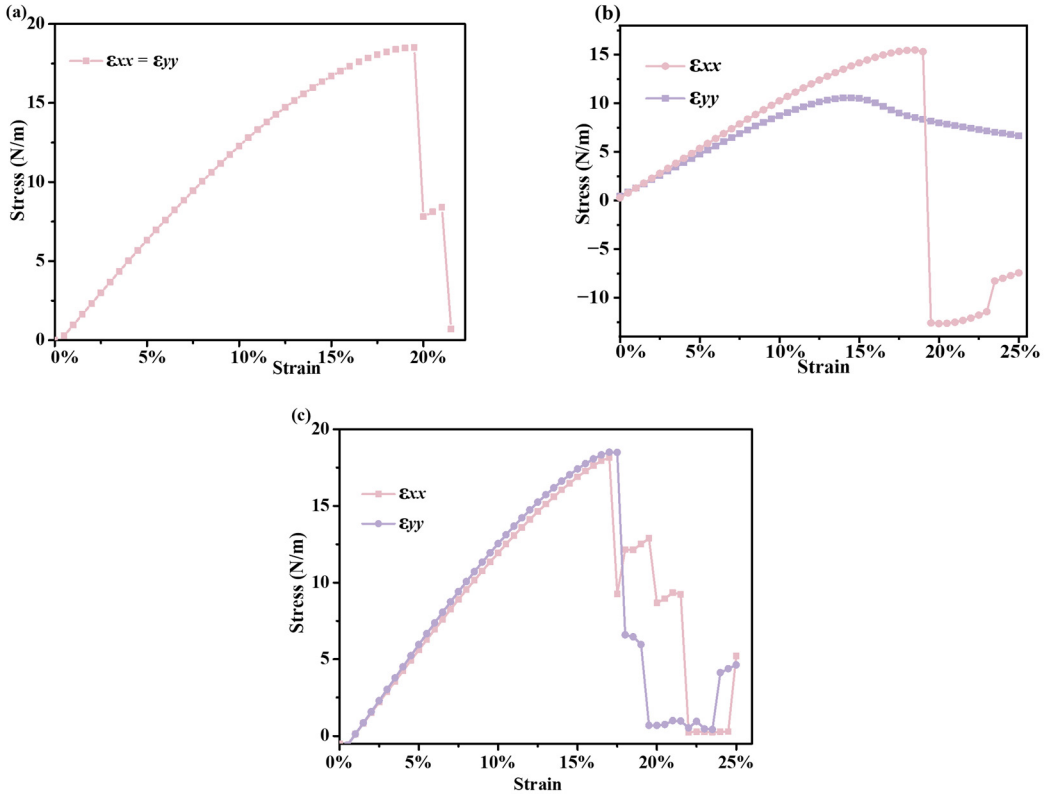

Figure 5. Strain–stress curves for the uniaxial tensile strains of B_6N_6 (**a**), B_5N_6Al (**b**), and B_5N_6C (**c**).

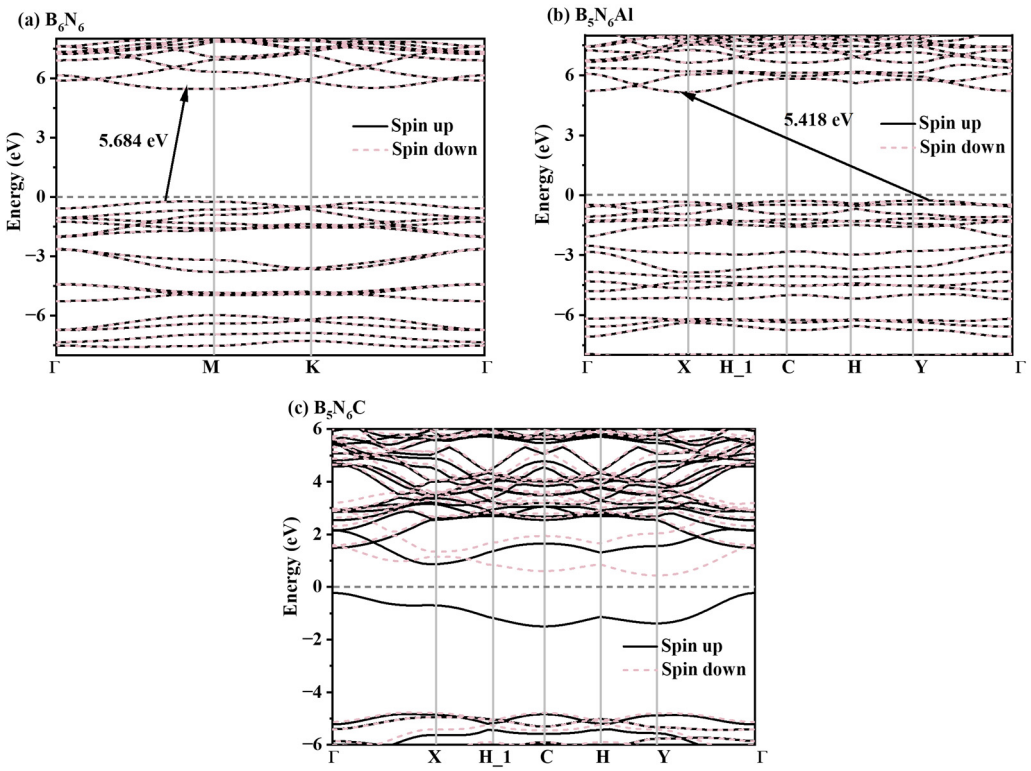

Figure 6. Electronic band structures of B_6N_6 (**a**), B_5N_6Al (**b**), and B_5N_6C (**c**). Black and red lines in the band structure present spin-up electrons and spin-down electrons, respectively.

We then explored the electronic properties of B_6N_6, B_5N_6Al, and B_5N_6C sheets by using the density of states (DOSs) and band decomposition charge density (BDCD) at the CBM and VBM. To verify the magnetism of these materials, their spin-up and spin-down

DOSs were simulated and are shown in Figure 7. For B_6N_6 sheet, the spin-up and spin-down density of states of N and B atoms are the same. In the energy range of 0~−20 eV, the contribution of N atoms is more than that of B atoms. In 5~10 eV, the contribution of the energy band is mainly from B atoms, that is, the conduction band is mainly contributed by N atoms, while the valence band is mainly contributed by B atoms. After doping with Al atoms, the spin-up and spin-down DOSs of nitrogen, boron, and aluminum atoms are also the same. It can be seen that the electrons contributed by Al atoms have always been the least, which may be due to the smallest proportion of Al atoms. At 0~−20 eV, N atoms contribute the most, which is similar to B_6N_6. At 5~8 eV, electrons mainly come from B atoms, while after doping with carbon atoms, both boron, nitrogen, and carbon atoms in B_5N_6C sheet exhibit differences, which indicates that B_5N_6C has a modicum of magnetism. For B_5N_6C sheet, the spin-up electrons come from B and C atoms in the energy window of −2~0 eV, which indicates that the narrowing of the spin-up band gap is mainly due to B and C atoms, independent of N atoms. In the energy ranges of −3~−27 eV and 0~5 eV, the N atom contributes the most to the electronic band, while at 5~10 eV, and the electrons are mainly derived from the B atom.

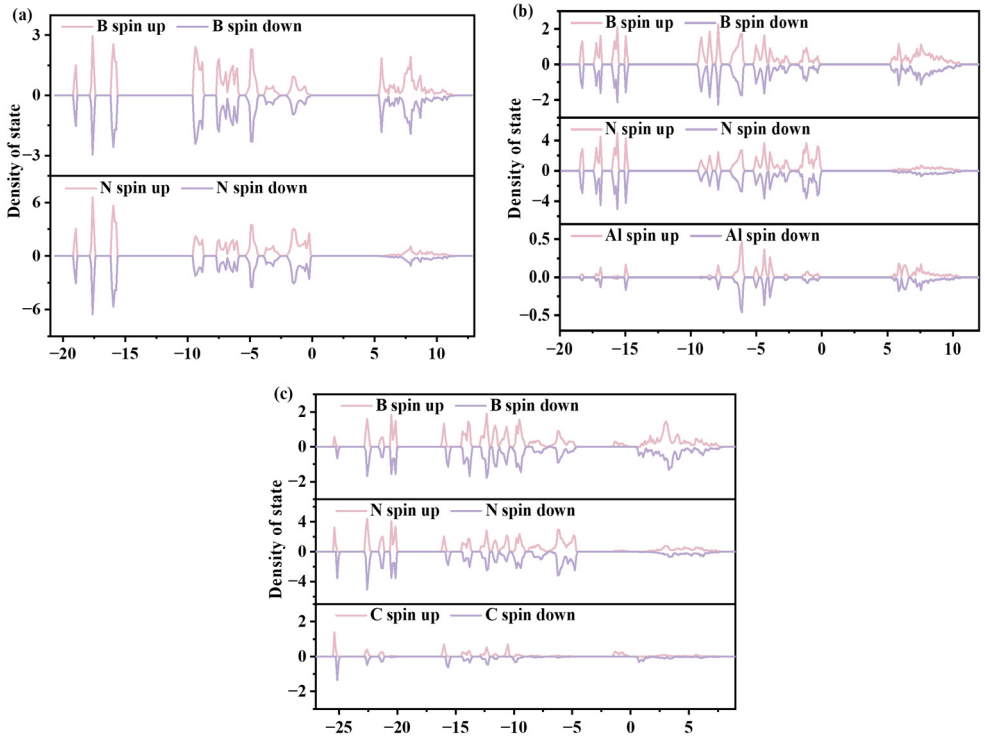

Figure 7. Spin-up and spin-down density of states for B_6N_6 (**a**), B_5N_6Al (**b**), and B_5N_6C (**c**).

The band decomposed charge densities (BDCDs) at the CBM and VBM of B_6N_6, B_5N_6Al, and B_5N_6C sheets are shown in Figure 8. As shown in the BDCDs, the electrons at the VBM of B_6N_6 sheet are mainly from the B atom, while the electrons at the CBM are mainly from the N atom. With the doping of Al atoms, the main contribution atoms of the CBM and VBM have reversed from before doping, while the Al atoms have no contribution to the CBM and VBM. For B_5N_6Al sheet, the VBM of B_5N_6Al sheet mainly comes from N atoms, and the CBM of B_6N_6 sheet mainly comes from B atoms. However, with the addition of the C atom, the distribution of electrons near the B_5N_6C sheet's CBM and VBM is irregular compared to that of the previous B_6N_6 sheet and B_5N_6Al sheet. After doping the C atom, the main contribution of the CBM and VBM is participated by doped atoms, but this also occurs mainly by nitrogen and boron atoms. In addition, the charge density at the spin-up VBM and CBM is also significantly different from that at the spin-down VBM and CBM. The charge at the spin-up VBM is mainly contributed by B and C atoms, while

the charge at the spin-down VBM is mainly contributed by N atoms. More rarely, negative charge appears at the spin-down CBM, as shown in the green part of Figure 8c.

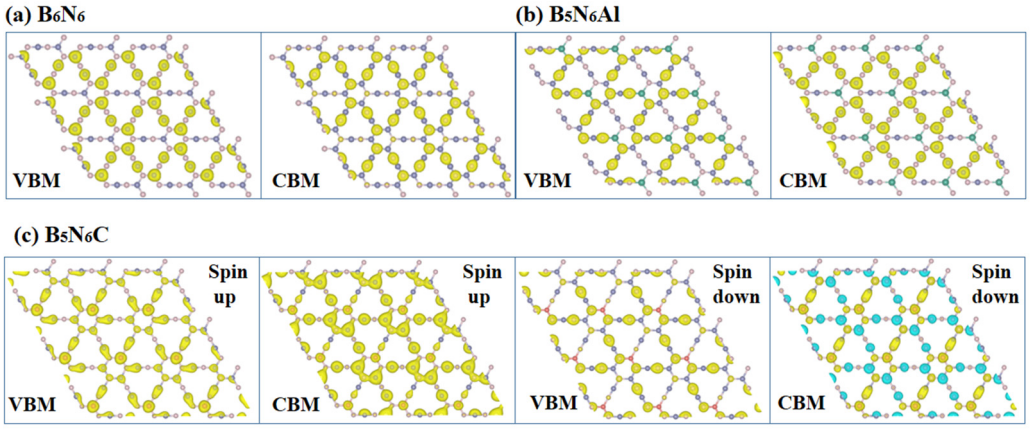

Figure 8. The band decomposed charge densities at the CBM and VBM of B_6N_6 (**a**), B_5N_6Al (**b**), and B_5N_6C (**c**).

Figure 9 illustrates the electron localization function (ELF) of B_6N_6, B_5N_6Al, and B_5N_6C. The electrons are well localized around the B-N bond, Al-N bond, and C-N bond. The strength of the covalent bond in B_6N_6 and B_5N_6Al sheets is similar, indicating that the doping of Al does not have a significant effect on the ELF. Compared with B_6N_6, the electron localization function of B_5N_6C is weaker. For B_5N_6C, the difference between the spin-up and spin-down ELF is less evident, but they are not exactly the same. Careful observation shows that the spin-down charge is slightly more than the spin-up charge. The magnetization direction for each atom of B_5N_6C is shown in Figure 10, where the blue arrow represents spin-up, and the red arrow represents spin-down. Both B and C atoms are spin-up, while N atoms are spin-down.

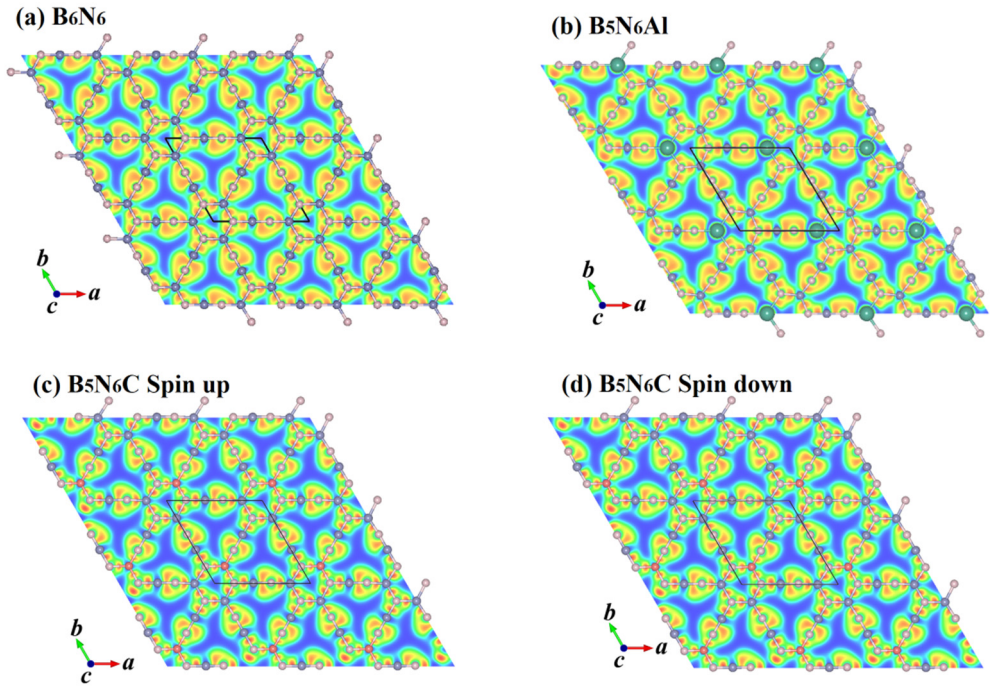

Figure 9. The electron localization function (ELF) of B_6N_6 (**a**), B_5N_6Al (**b**), and B_5N_6C (**c**,**d**).

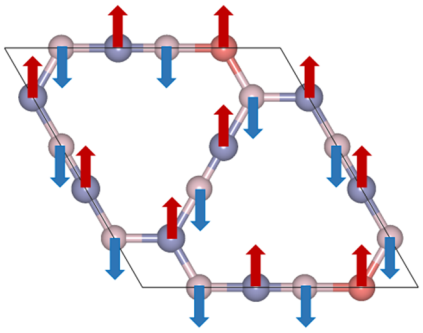

Figure 10. The magnetization direction for each atom of B_5N_6C; arrows denote spins.

3. Materials and Methods

The prediction of all the geometric optimization and properties of B_6N_6, B_5N_6Al, and B_5N_6C in this article was made on the basis of the first-principles calculation of the density functional theory (DFT) implemented in Mede A and VASP (3.3) [38,39]. The cutoff energy was selected to be 500 eV for plane waves. Electron–ion interactions were represented with the projector augmented wave (PAW) [40] pseudopotentials. The generalized gradients approximation proposed by the Perdew–Burke–Ernzerhof (GGA-PBE) functional is employed for the exchange correlation potential [41]. In order to fully optimize the geometry of the unit cell, the total energy convergence was set to 1×10^{-8} eV, and the atomic convergence force was 0.001 eV/Å. The Brillouin zone was sampled with an $8 \times 8 \times 1$ Monkhorst–Pack (MP) [42] special k-point grid for geometric optimization and properties prediction. The hybrid Heyd–Scuseria–Ernzerhof functional (HSE06) [43] was used to simulate the band structures. In order to verify the mechanical stability, the elastic constants of B_6N_6, B_5N_6Al, and B_5N_6C sheets were estimated in vaspkit (1.4.0) [44] using the energy–strain method.

4. Conclusions

Based on density functional theory, we studied the electronic properties, mechanical properties, anisotropy properties, and magnetic properties of B_6N_6, B_5N_6Al, and B_5N_6C sheets. B_6N_6, B_5N_6Al, and B_5N_6C sheets are all composed of six-membered rings and twelve-membered rings. All the B_6N_6, B_5N_6Al, and B_5N_6C sheets are anisotropic materials, and B_6N_6 sheet has the largest anisotropy in terms of Young's modulus and Poisson's ratio. B_6N_6 and B_5N_6C sheets have good mechanical properties compared to B_5N_6Al sheet, making them suitable for nanomechanical applications. B_6N_6 and B_5N_6Al sheets have indirect band gaps of 5.684 and 5.418 eV, respectively. Therefore, by calculating the spin-up and spin-down band structures, it was found that B_6N_6 sheet did not exhibit magnetic properties. With the insertion of aluminum atoms, B_5N_6Al sheet also did not show magnetism. However, with the doping of carbon atoms, B_5N_6C sheet shows a modicum of magnetism, and all three atoms (B atom, N atom, and C atom) that were not magnetic atoms themselves showed magnetism.

Author Contributions: Conceptualization, L.Q.; methodology, L.Q.; software, L.Q.; validation, Z.M.; formal analysis, Z.M.; investigation, F.Y.; resources, Q.F.; data curation, F.Y.; writing—original draft preparation, Q.F.; writing—review and editing, S.W.; visualization, S.W.; supervision, L.Q.; project administration, Q.F.; funding acquisition, L.Q. All authors have read and agreed to the published version of the manuscript.

Funding: This work was supported by the National Natural Science Foundation of China (Nos. 62164011 and 61804120), China Postdoctoral Science Foundation (Nos. 2019TQ0243, 2019M663646), the Natural Science Basic Research Program of Shaanxi Province (No. 2023-JC-YB-567), Key Science and Technology Innovation Team of Shaanxi Province (2022TD-34), the Natural Science Foundation of Jiangsu Province (No. BK20211002), as well as Qinglan Project of Jiangsu Province of China.

Data Availability Statement: Data are contained within the article.

Conflicts of Interest: The authors declare no conflicts of interest.

References

1. Bi, J.X.; Du, Z.Z.; Sun, J.M.; Liu, Y.H.; Wang, K.; Du, H.F.; Ai, W.; Huang, W. On the Road to the Frontiers of Lithium-Ion Batteries: A Review and Outlook of Graphene Anodes. *Adv. Mater.* **2023**, *35*, e2210734. [CrossRef]
2. Olabi, A.G.; Abdelkareem, M.A.; Wilberforce, T.; Sayed, E.T. Application of graphene in energy storage device—A review. *Renew. Sust. Energ. Rev.* **2021**, *135*, 110026. [CrossRef]
3. Xiao, Y.Q.; Pang, Y.X.; Yan, Y.X.; Qian, P.; Zhao, H.T.; Manickam, S.; Wu, T.; Pang, C.H. Synthesis and Functionalization of Graphene Materials for Biomedical Applications: Recent Advances, Challenges, and Perspectives. *Adv. Sci.* **2023**, *10*, e2205292. [CrossRef]
4. Yang, H.B.; Zheng, H.J.; Duan, Y.X.; Xu, T.; Xie, H.X.; Du, H.S.; Si, C.L. Nanocellulose-graphene composites: Preparation and applications in flexible electronics. *Int. J. Biol. Macromol.* **2023**, *253*, 126903. [CrossRef]
5. Ghosa, S.; Mondal, N.S.; Chowdhury, S.; Jana, D. Two novel phases of germa-graphene: Prediction, electronic and transport applications. *Appl. Surf. Sci.* **2023**, *614*, 156107. [CrossRef]
6. Asim, N.; Badiei, M.; Samsudin, N.A.; Mohammad, M.; Razali, H.; Soltani, S.; Amin, N. Application of graphene-based materials in developing sustainable infrastructure: An overview. *Compos. B. Eng.* **2022**, *245*, 110188. [CrossRef]
7. Sun, M.; Chou, J.P.; Hu, A.; Schwingenschlögl, U. Point Defects in Blue Phosphorene. *Chem. Mater.* **2019**, *31*, 8129–8135. [CrossRef]
8. Ma, Y.; Yan, Y.; Luo, L.; Pazos, S.; Zhang, C.; Lv, X.; Chen, M.; Liu, C.; Wang, Y.; Chen, A.; et al. High-performance van der Waals antiferroelectric CuCrP2S6-based memristors. *Nat. Commun.* **2023**, *14*, 7891. [CrossRef]
9. Zhang, C.; Ren, K.; Wang, S.; Luo, Y.; Tang, W.; Sun, M. Recent progress on two-dimensional van der Waals heterostructures for photocatalytic water splitting: A selective review. *J. Phys. D Appl. Phys.* **2023**, *56*, 483001. [CrossRef]
10. Zhang, W.; Chai, C.; Fan, Q.; Yang, Y.; Sun, M.; Palummo, M.; Schwingenschlögl, U. Two-dimensional borocarbonitrides for photocatalysis and photovoltaics. *J. Mater. Chem. C* **2023**, *11*, 3875–3884. [CrossRef]
11. Ren, K.; Yan, Y.; Zhang, Z.; Sun, M.; Schwingenschlogl, U. A family of LixBy monolayers with a wide spectrum of potential applications. *Appl. Surf. Sci.* **2022**, *604*, 154317. [CrossRef]
12. Sun, M.; Re Fiorentin, M.; Schwingenschlögl, U.; Palummo, M. Excitons and light-emission in semiconducting $MoSi_2X_4$ two-dimensional materials. *NPJ 2D Mater. Appl.* **2022**, *6*, 81. [CrossRef]
13. Wang, Y.; Miao, M.; Lv, J.; Zhu, L.; Yin, K.; Liu, H.; Ma, Y. An Effective Structure Prediction Method for Layered Materials Based on 2D Particle Swarm Optimization Algorithm. *J. Chem. Phys.* **2012**, *137*, 224108–224114. [CrossRef]
14. Pakdel, A.; Bando, Y.; Golberg, D. Nano boron nitride flatland. *Chem. Soc. Rev.* **2014**, *43*, 934–959. [CrossRef]
15. Entani, S.; Larionov, K.V.; Popov, Z.I.; Takizawa, M.; Mizuguchi, M.; Watanabe, H.; Li, S.T.; Naramoto, H.; Sorokin, P.B.; Sakai, S. Non-chemical fluorination of hexagonal boron nitride by high-energy ion irradiation. *Nanotechnology* **2020**, *31*, 125705. [CrossRef] [PubMed]
16. Wang, J.G.; Mu, X.J.; Wang, X.X.; Wang, N.; Ma, F.C.; Liang, W.J.; Sun, M.T. The thermal and thermoelectric properties of in-plane C-BN hybrid structures and graphene/h-BN van der Waals heterostructures. *Mater. Today Phys.* **2018**, *5*, 29–57. [CrossRef]
17. Sun, M.; Tang, W.; Ren, Q.; Wang, S.; Yu, J.; Du, Y. A first-principles study of light non-metallic atom substituted blue phosphorene. *Appl. Surf. Sci.* **2015**, *356*, 110–114. [CrossRef]
18. Wang, Z.H.; Zhou, X.F.; Zhang, X.M.; Zhu, Q.; Dong, H.F.; Zhao, M.W.; Oganov, A.R. Phagraphene: A Low-Energy Graphene Allotrope Composed of 5–6-7 Carbon Rings with Distorted Dirac Cones. *Nano Lett.* **2015**, *15*, 6182–6186. [CrossRef] [PubMed]
19. Singh, N.B.; Bhattacharya, B.; Sarkar, U. A first principle study of pristine and BN-doped graphyne family. *Struct. Chem.* **2014**, *25*, 1695–1710. [CrossRef]
20. Enyashin, A.N.; Ivanovskii, A.L. Graphene-like BN allotropes: Structural and electronic properties from DFTB calculations. *Chem. Phys. Lett.* **2011**, *509*, 143–147. [CrossRef]
21. Bu, H.; Zhao, M.; Zhang, H.; Wang, X.; Xi, Y.; Wang, Z. Isoelectronic Doping of Graphdiyne with Boron and Nitrogen: Stable Configurations and Band Gap Modification. *J. Phys. Chem. A* **2012**, *116*, 3934–3939. [CrossRef]
22. Shahrokhi, M.; Mortazavi, B.; Berdiyorov, R.G. New two-dimensional Boron Nitride allotropes with attractive electronic and optical properties. *Solid State Commun.* **2017**, *253*, 51–56. [CrossRef]
23. Demirci, S.; Rad, S.E.; Kazak, S.; Nezir, S.; Jahangirov, S. Monolayer diboron dinitride: Direct band-gap semiconductor with high absorption in the visible range. *Phys. Rev. B* **2020**, *101*, 125408. [CrossRef]
24. Li, X.D.; Cheng, X.L. Predicting the structural and electronic properties of two-dimensional single layer boron nitride sheets. *Chem. Phys. Lett.* **2018**, *694*, 102–106. [CrossRef]
25. Chen, Y.; Zou, J.; Campbell, S.J.; Le Caer, G. Boron nitride nanotubes: Pronounced resistance to oxidation. *Appl. Phys. Lett.* **2004**, *84*, 2430–2432. [CrossRef]
26. Wang, X.; Zhi, C.; Li, L.; Zeng, H.; Li, C.; Mitome, M.; Golberg, D.; Bando, Y. "Chemical Blowing" of Thin-Walled Bubbles: High-Throughput Fabrication of Large-Area, Few-Layered BN and C_x-BN Nanosheets. *Adv. Mater.* **2011**, *23*, 4072–4076. [CrossRef] [PubMed]
27. Zhi, C.; Bando, Y.; Tang, C.; Kuwahara, H.; Golberg, D. Large-Scale Fabrication of Boron Nitride Nanosheets and Their Utilization in Polymeric Composites with Improved Thermal and Mechanical Properties. *Adv. Mater.* **2009**, *21*, 2889–2893. [CrossRef]
28. Anota, E.C.; Hernández, A.B.; Morales, A.E.; Castro, M. Design of the magnetic homonuclear bonds boron nitride nanosheets using DFT methods. *J. Mol. Graph. Model.* **2017**, *74*, 135–142. [CrossRef]

29. Cao, X.; Li, Y.; Cheng, X.; Zhang, Y. Structural analogues of graphyne family: New types of boron nitride sheets with wide band gap and strong UV absorption. *Chem. Phys. Lett.* **2011**, *502*, 217–221. [CrossRef]
30. Qi, J.; Wang, S.; Wang, J.; Umezawa, N.; Blatov, V.A.; Hosono, H. B_5N_3 and B7N5 Monolayers with High Carrier Mobility and Excellent Optical Performance. *J. Phys. Chem. Lett.* **2021**, *12*, 4823–4832. [CrossRef]
31. Hohenberg, P.; Kohn, W. Inhomogeneous electron gas. *Phys. Rev.* **1964**, *136*, B864. [CrossRef]
32. Kohn, W.; Sham, L.J. Self-consistent equations including exchange and correlation effects. *Phys. Rev.* **1956**, *140*, A1133. [CrossRef]
33. Fan, Q.; Zhou, H.; Zhao, Y.; Yun, S. Predicting a novel two-dimensional BN material with a wide band gap. *Energy Mater.* **2022**, *2*, 200022. [CrossRef]
34. Anota, E.C. 2D boron nitride incorporating homonuclear boron bonds: Stabilized in neutral, anionic and cationic charge. *SN Appl. Sci.* **2022**, *4*, 295. [CrossRef]
35. Cadelano, E.; Palla, P.L.; Giordano, S.; Colombo, L. Elastic properties of hydrogenated graphene. *Phys. Rev. B* **2010**, *82*, 235414. [CrossRef]
36. Ding, Y.; Wang, Y. Density functional theory study of the silicene-like SiX and XSi_3 (X = B, C, N, Al, P) honeycomb lattices: The various buckled structures and versatile electronic properties. *J. Phys. Chem. C* **2013**, *117*, 18266–18278. [CrossRef]
37. Andrew, R.C.; Mapasha, R.E.; Ukpong, A.M.; Chetty, N. Mechanical properties of graphene and boronitrene. *Phys. Rev. B* **2012**, *85*, 125428. [CrossRef]
38. Kresse, G.; Furthmüller, J. Efficiency of ab initio total energy calculations for metals and semiconductors using a plane-wave basis set. *Comput. Mater. Sci.* **1996**, *6*, 15–50. [CrossRef]
39. Kresse, G.; Furthmüller, J. Efficient iterative schemes for ab initio total-energy calculations using a plane-wave basis set. *Phys. Rev. B* **1996**, *54*, 11169–11186. [CrossRef] [PubMed]
40. Blöchl, P.E. Projector augmented-wave method. *Phys. Rev. B* **1994**, *50*, 17953. [CrossRef] [PubMed]
41. Perdew, J.P.; Burke, K.; Ernzerhof, M. Generalized gradient approximation made simple. *Phys. Rev. Lett.* **1996**, *77*, 3865. [CrossRef] [PubMed]
42. Monkhorst, H.J.; Pack, J.D. Special points for brillouinzone integrations. *Phys. Rev. B* **1976**, *13*, 5188. [CrossRef]
43. Krukau, A.V.; Vydrov, O.A.; Izmaylov, A.F.; Scuseria, G.E. Influence of the exchange screening parameter on the performance of screened hybrid functionals. *J. Chem. Phys.* **2006**, *125*, 224106. [CrossRef] [PubMed]
44. Wang, V.; Liu, J.C.; Tang, G.; Geng, W.T. VASPKIT: A user-friendly interface facilitating high-throughput computing and analysis using VASP code. *Comput. Phys. Commun.* **2021**, *267*, 108033. [CrossRef]